CrystEngComm

PAPER

View Article Online
View Journal | View Issue

Cite this: *CrystEngComm*, 2017, **19**, 4273

Novel drug–drug cocrystals of carbamazepine with *para*-aminosalicylic acid: screening, crystal structures and comparative study of carbamazepine cocrystal formation thermodynamics†‡

Ksenia V. Drozd,[a] Alex N. Manin, [a] Andrei V. Churakov[b] and German L. Perlovich *[a]

The cocrystal formation of the anticonvulsant drug carbamazepine (CBZ) with *para*-aminosalicylic acid (PASA, antituberculous drug) has been studied by varying the molar ratios of CBZ to PASA (1 : 1 and 2 : 1) and using liquid-assisted grinding (LAG), slurrying and solution crystallization methods. Three novel cocrystal forms of CBZ and PASA have been synthesized: [CBZ + PASA] (1 : 1), [CBZ + PASA + H_2O] (2 : 1 : 1) and [CBZ + PASA + MeOH] (2 : 1 : 1), and their crystal structures have been described. Conformational analysis of the CBZ molecule in its polymorphic forms, its cocrystals and solvates has been conducted. Calculations of intermolecular interaction energies using the PIXEL approach have been carried out for CBZ cocrystals with 1 : 1 stoichiometry. The melting and desolvation processes of the [CBZ + PASA] (1 : 1), [CBZ + PASA + H_2O] (2 : 1 : 1) and [CBZ + PASA + MeOH] (2 : 1 : 1) cocrystals have been studied. The temperature dependence of the CBZ (form III) saturation vapor pressure has been studied, and the sublimation thermodynamic functions have been calculated. Based on the sublimation thermodynamics database of molecular crystals, the standard sublimation thermodynamic functions of PASA have been evaluated. The thermodynamic functions of cocrystal formation based on CBZ have been calculated and analyzed. The dissolution process of the [CBZ + PASA] cocrystal (1 : 1) in water (pH 7.4) has been studied. CBZ cocrystallization with PASA has been shown to lead to a dramatic decrease of the CBZ rate of conversion from the anhydrous to the hydrate form, and as a consequence, to solubility improvement by approximately 1.5 times.

Received 3rd May 2017,
Accepted 23rd June 2017

DOI: 10.1039/c7ce00831g

rsc.li/crystengcomm

Introduction

Today, the approach of combining several drugs to treat many serious diseases (such as virulent diseases, HIV/AIDS, cancer, diabetes, cardiovascular diseases) definitely forces out monotherapy (aimed at a definite receptor).[1] The use of cost-effective and multi-target fixed-dose drug combinations (FDC) can help reduce the pill load without the additional risk of adverse events or drug resistance, thereby improving patient compliance by simplified disease management.[2] An alternative approach to using drug combinations is the use of multi-component crystals such as salts, complexes, and cocrystals containing more than one active pharmaceutical ingredient.[3] Among all the mentioned multi-component systems, cocrystals attract the biggest attention of the pharmaceutical industry[4] due to the introduction of regulatory guidelines by the US Food and Drug Administration (FDA)[5] as a result of expanded patent portfolios.[2] Unfortunately, cocrystal studies mainly focus on crystal engineering and supramolecular synthesis of API-based cocrystals. For example, the pharmaceutical properties have not been evaluated for the [sulfadimidine + aspirin] cocrystal[6] which can be regarded as an antibacterial and an NSAID therapeutic drug. Another example is the two-component crystal of piracetam (a nootropic agent) with gentisic acid (NSAID),[7] for which no studies have been conducted except those of the synthons' nature in the cocrystal formation. The study of drug–drug cocrystals in terms of their further use in the pharmaceutical industry is much less intensive,[8,9] though designing drug–drug

[a] *G.A. Krestov Institute of Solution Chemistry of the Russian Academy of Sciences, 1, Akademicheskaya St., 153045, Ivanovo, Russia. E-mail: glp@isc-ras.ru; Fax: +7 4932 336237; Tel: +7 4932 533784*
[b] *Institute of General and Inorganic Chemistry RAS, Leninsky Prosp. 31, 119991 Moscow, Russia*

† The authors declare no competing financial interest.

‡ Electronic supplementary information (ESI) available: XRPD patterns of samples obtained by slurrying and from dissolution experiments, DSC/TG thermograms, estimation of sublimation thermodynamic functions, conformational analysis of polymorphs of CBZ and its cocrystals, hydrogen bond details and CIFs. CCDC 1544195–1544197. For ESI and crystallographic data in CIF or other electronic format see DOI: 10.1039/c7ce00831g

cocrystals of marketed drugs may shorten the development period (including clinical trials) compared to those of New Chemical Entities, as cocrystals do not involve structural modification of the APIs.[10]

Carbamazepine (CBZ) is an anticonvulsant and a mood-stabilizing drug used primarily to treat epilepsy, bipolar disorder and trigeminal neuralgia (Fig. 1). According to the biopharmaceutical classification system, carbamazepine is classified as a class II drug[11] having low water solubility which limits its absorption. CBZ cocrystallization with more soluble coformers is one of the solutions to this problem.[12] The Cambridge Structural Database (CSD) so far contains over 50 crystalline forms of CBZ, most of which are cocrystals, including drug–drug cocrystals, as well as their solvates/hydrates and polymorphs.[13]

The purpose of our research was to obtain and study drug–drug carbamazepine cocrystals with antituberculosis drugs. Recent studies have shown that pharmacological stimulation of autophagy by carbamazepine avoids the immunosuppressive effects of *m*TOR inhibition seen with rapamycin, promoting both innate and adaptive immune responses to mycobacterial infection and proves the concept for a novel therapeutic strategy unaffected by bacterial resistance to conventional antibiotics.[14] Earlier, Swart A. and Harris V.[15] reported on the CBZ interaction with first-line antituberculosis drugs: isoniazid and rifampicin. According to this report, their simultaneous administration leads to serious side effects. Therefore, *para*-aminosalicylic acid (PASA), a second-line antituberculosis drug, was chosen for cocrystallization with CBZ (Fig. 1).

In this context, we conducted cocrystal screening of carbamazepine with *para*-aminosalicylic acid. The cocrystals and their solvates were characterized by single crystal X-ray diffraction and differential scanning calorimetry. The cocrystal aqueous dissolution and solution stability were also investigated. In addition, analysis of the intermolecular interaction and crystal lattice energies of the carbamazepine cocrystals was performed using the PIXEL approach.

One of the most important fundamental problems of cocrystallization studies is the prediction of the stability of the new cocrystal . An approach is proposed for estimating the thermodynamic parameters of the cocrystal formation based on the thermodynamic functions of the components of known CBZ cocrystals.

Carbamazepine (CBZ) *para*-Aminosalicylic acid (PASA)

Fig. 1 Molecular structures of carbamazepine and *para*-aminosalicylic acid. The flexible torsion angle in carbamazepine is numbered and is indicated by τ.

Materials and methods

Compounds and solvents

Carbamazepine was purchased from Acros Organics while *para*-aminosalicylic acid was supplied by Sigma-Aldrich. All the compounds were used without further purification. Analytical grade solvents were used for the crystallization experiments.

Cocrystal preparation

Synthesis *via* grinding. The grinding was performed using a Fritsch planetary micro mill model Pulverisette 7 with 12 ml agate grinding jars and ten 5 mm agate balls at a rate of 500 rpm for 30 min. The experiments were carried out with 1 : 1 and 2 : 1 stoichiometries of CBZ and PASA (the total physical mixture weight was *ca.* 50 mg). Solvent-drop grinding experiments were conducted prior to the grinding by adding *ca.* 0.05 ml of the solvent to the reactants using a micropipette. The resulting powder samples were analyzed by PXRD for the cocrystal formation.

Synthesis *via* slurrying. Approximately 50 mg of CBZ with PASA in 1 : 1 and 2 : 1 stoichiometries were mixed in a 2 mL test tube with the solvent amount sufficient to produce a wet paste. The mixture was sonicated at room temperature for 15–20 min at maximum power.[16] The resulting solids were air-dried prior to subsequent analysis.

Solution crystallization

A slow evaporation method was used to grow single crystals. Cocrystallization experiments were carried out by dissolving 80 mg of either a 1 : 1 or a 2 : 1 mixture of CBZ and PASA in a minimum amount of the solvent selected from acetonitrile (ACN), acetone (AO), ethanol (EtOH), methanol (MeOH), tetrahydrofuran (THF) and ethyl acetate ($EtOCH_3$). The vials containing the dissolved mixtures were covered with a parafilm, punctured with 3–5 holes and allowed to slowly evaporate under ambient conditions. The crystallization experiment results are given below (Table 1).

Table 1 Results of CBZ and PASA crystallization from different solvents

Solvent	Molar ratio	[CBZ + PASA] (1 : 1)	[CBZ + PASA + H_2O] (2 : 1 : 1)	[CBZ + PASA + MeOH] (2 : 1 : 1)
ACN	1 : 1	Yes	—	—
	2 : 1	—	Yes	—
MeOH	1 : 1	—	—	Yes
	2 : 1	—	—	—
EtOH	1 : 1	—	—	—
	2 : 1	—	—	—
THF	1 : 1	Yes	—	—
	2 : 1	Yes	—	—
AO	1 : 1	—	—	—
	2 : 1	—	—	—
$EtOCH_3$	1 : 1	—	Yes	—
	2 : 1	—	—	—

Single crystal X-ray diffraction

Single-crystal X-ray diffraction data were collected using a Bruker SMART APEX II diffractometer with graphite-monochromated Mo-Kα radiation (λ = 0.71073 Å) in the ω-scan mode. Absorption corrections based on measurements of equivalent reflections were applied.[17] The structures were solved by direct methods and refined by full matrix least-squares on F^2 with anisotropic thermal parameters for all the non-hydrogen atoms.[18] All hydrogen atoms were found from a difference Fourier map and refined with isotropic thermal parameters.

Powder X-ray diffraction (PXRD)

X-ray powder diffraction data were recorded under ambient conditions in Bragg–Brentano geometry on a Bruker D8 Advance diffractometer with Cu Kα radiation (λ = 1.5406 Å) at 40 kV and 40 mA power. The X-ray diffraction patterns were collected over the 2θ range 5–30°, with a 0.03° step size.

Crystal lattice energy calculations

Intermolecular interaction energies were calculated using the PIXEL approach developed by Gavezzotti.[19,20] This method provides quantitative determination of crystal lattice energies and pairwise intermolecular interactions, with a breakdown of these energies into Coulombic, polarization, dispersion and repulsion terms. The molecular electron densities for the cocrystals were calculated at the MP2/6-31G** level of theory in the GAUSSIAN09 program. All the hydrogen atoms in the structures were set to the standard neutron values according to the default procedure in the PIXEL program.

Differential scanning calorimetry (DSC)

DSC was performed using a Perkin Elmer DSC 4000 differential scanning calorimeter with a refrigerated cooling system (USA). The sample was heated in sealed aluminum sample holders from 30 to 210 °C at a heating rate of 10 °C min^{-1} in a nitrogen atmosphere. The unit was calibrated with indium and zinc standards. The accuracy of the weighing procedure was ±0.01 mg.

Thermogravimetric analysis (TGA)

TGA was performed using a TG 209 F1 Iris thermomicrobalance (Netzsch, Germany). Approximately 10 mg of the sample was put in a platinum crucible. The samples were heated over the temperature range of 30 to 210 °C at a heating rate of 10 °C min^{-1}. The samples were purged with a stream of flowing dry Ar at 30 ml min^{-1} throughout the experiment.

Sublimation measurements

The sublimation experiments were carried out by the transpiration method as described elsewhere.[21,22] In brief, a stream of an inert gas passes above the sample at a constant temperature and at a known slow constant flow rate in order to achieve saturation of the carrier gas with the vapor of the substance under investigation. The vapor is condensed at some point downstream, and the mass of the sublimate and its purity are determined by UV-Vis spectrophotometry and DSC. The vapor pressure over the sample at this temperature can be calculated by means of the amount of the sublimated sample and the volume of the inert gas used.

Aqueous dissolution experiment

The dissolution measurements were made by the shake-flask method in phosphate buffer with pH 7.4 at 25.0 ± 0.1 °C for 6 h. An excess amount of the sample was suspended in the respective buffer solution in Pyrex glass tubes. The dissolved drug amount was measured by taking aliquots of the media. The suspension was filtered through a 0.2 μm PTEF syringe filter (Rotilabo), and the concentration was determined by high-performance liquid chromatography (HPLC). HPLC was conducted on a Shimadzu Prominence model LC-20 AD equipped with a PDA detector and a C-18 column (150 mm × 4.6 mm i.d., 5 μm particle size and 100 Å pore size). The elution was achieved by a mobile phase consisting of 50% phosphate buffer pH 3.5 (A) and 50% methanol, and the flow rate was 0.5 mL min^{-1}. The concentration of the components was measured at the wavelength of 284 (CBZ) and 266 and 298 nm (PASA).

Results and discussion

Cocrystal production and preliminary identification

The initial stage of our research was to identify the formation of new crystalline species (cocrystal) between carbamazepine and *para*-aminosalicylic acid. The cocrystal formation feasibility was verified by the DSC and XRPD methods. At first the 1 : 1 molar ratio of the studied compounds was tested. The DSC curves for the individual components and the mixture after cogrinding are shown in Fig. 2a. The CBZ DSC thermogram represents the characteristic thermal events of CBZ form III (*p*-monoclinic): two endotherms and one exotherm (Fig. 2a), as reported by Grzesiak.[23] The DSC thermogram of the 1 : 1 mixture shows only one major endothermic event at 154.0 °C (onset), which differs from the melting points of both CBZ (191 °C) and PASA (139.1 °C). This indicates that during the cogrinding experiment, a new phase (cocrystal) was formed between CBZ and PASA. The XRPD patterns for CBZ, PASA and their 1 : 1 mixture are illustrated in Fig. 2b. The diffraction pattern of the ground mixture was found to be distinctly different (new peaks at 2θ angles of 9.7°, 12.5°, 14.9°, 16.7°, 17.7°, 18.3°, 19.3°, 21.3° and 28.3°) as compared to the starting compounds, indicating the formation of a new solid, *i.e.* a cocrystal.

There are known cases when some compounds (which include APIs) can form cocrystals in multiple stoichiometries with the same coformer: [CBZ + *para*-aminobenzoic acid (PABA)] (1 : 1, 2 : 1 and 4 : 1),[24,25] [caffeine + maleic acid] (1 : 1

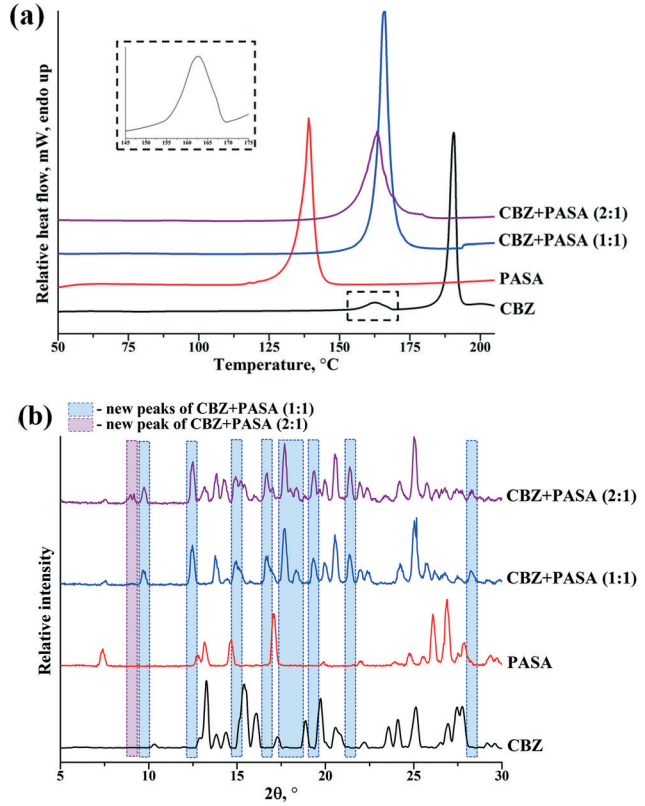

Fig. 2 (a) DSC heating curves and (b) experimental XRPD patterns of pure carbamazepine (black), *para*-aminosalicylic acid (red), and 1 : 1 (blue) and 2 : 1 (purple) mixtures of compounds after cogrinding.

and 2 : 1),[26,27] [nicotinamide + (*R*)-mandelic acid] (1 : 1, 4 : 1 and 1 : 2)[28] and others. Consequently, the 2 : 1 molar ratio with an excess of CBZ was additionally tested. The DSC curves and XRPD patterns of the 2 : 1 mixture prepared by grinding are shown in Fig. 2 *versus* the starting components and cocrystal in a 1 : 1 molar ratio. The DSC thermogram of the 2 : 1 mixture shows a broad and low melting peak at 153.4 °C (onset) *versus* the sharp peak of the 1 : 1 cocrystal. The XRPD pattern of the 2 : 1 mixture presents the peaks of the 1 : 1 cocrystal, CBZ and the new double peak at 9° 2θ. Thus, the carbamazepine cocrystal with *para*-aminosalicylic acid can be produced by grinding the compounds in 1 : 1 or 2 : 1 stoichiometries. Moreover, the cocrystal formation leads to a *ca.* 30 °C decrease in the melting point compared to the pure CBZ.

Screening by slow crystallization from the solution was the next stage of the investigation. The experiment was carried out by using six different solvents. All the single crystals of carbamazepine cocrystals with *para*-aminosalicylic acid were obtained by slow evaporation (Table 1). Colorless crystalline materials were obtained within 5 days. As a result, we produced single crystals of [CBZ + PASA] (1 : 1), [CBZ + PASA + H_2O] (2 : 1 : 1) and [CBZ + PASA + MeOH] (2 : 1 : 1). Unfortunately, the pure crystal form of the [CBZ + PASA] cocrystal (2 : 1) was not obtained.

Liquid-assisted grinding (LAG) and slurry experiments for [CBZ + PASA] cocrystallization discovery

The screening of [CBZ + PASA] crystals by slow crystallization from the solution has shown that there are at least 3 new forms: cocrystal (1 : 1), cocrystal methanol solvate (2 : 1 : 1) and cocrystal hydrate (2 : 1 : 1). Two methods were tested to obtain the required quantity of new cocrystal forms: cogrinding and slurrying.

The influence of liquid-assisted grinding and sonication conditions on the outcome of CBZ cocrystal forms was investigated by adding the solvent to the physical mixtures in 1 : 1 and 2 : 1 stoichiometries. The results of the experiment are summarized in Table 2.

The findings have revealed that the grinding of the 1 : 1 physical mixture with acetonitrile (ACN), acetone (AO), methanol (MeOH), ethanol (EtOH), tetrahydrofuran (THF), chloroform ($CHCl_3$) and water (H_2O) leads to [CBZ + PASA] (1 : 1) cocrystal formation. The neat grinding and grinding with ethyl acetate have produced a [CBZ + PASA] (1 : 1) cocrystal with a small amount of unconverted CBZ (Fig. 3).

A pure [CBZ + PASA + MeOH] (2 : 1 : 1) form was obtained only by grinding the compounds with an excess amount of CBZ with methanol. In the case of cogrinding of the 2 : 1 mixture with water, the unreacted CBZ was partially converted to the dihydrate form (Fig. 4).

It should be noted that no evidence of [CBZ + PASA + H_2O] (2 : 1 : 1) formation in any of the mechanochemical and slurry experiments (Fig. S1 and S2, see the ESI‡) has been found. Moreover, in comparison with the grinding experiments, CBZ and PASA slurrying in 1 : 1 and 2 : 1 stoichiometries more often leads to CBZ hydration (Table 2).

Crystal structure analysis

Diffraction quality single crystals of [CBZ + PASA] (1 : 1) were grown by slow evaporation of an acetonitrile or tetrahydrofuran solution at room temperature.

The solution was prepared by dissolving a mixture of CBZ and PASA in 1 : 1 and/or 2 : 1 molar ratios in the case of tetrahydrofuran. Single crystals of [CBZ + PASA] cocrystal monohydrate (2 : 1) were grown from acetonitrile by dissolving CBZ and PASA in a 2 : 1 molar ratio and from ethyl acetate in a 1 : 1 molar ratio. We were also able to obtain single crystals of the [CBZ + PASA] (2 : 1) methanol solvate which were crystallized from the methanol solution of CBZ and PASA mixture with 1 : 1 stoichiometry.

The crystallographic data for the cocrystals are summarized in Table 3, whereas the hydrogen bonding geometries are listed in Table S1 (see the ESI‡).

Carbamazepine/*para*-aminosalicylic acid 1 : 1 cocrystal (1). The colorless prism-shaped crystals grown from acetonitrile and tetrahydrofuran (Table 1) were found to belong to the monoclinic, *C*2/*c* space group (Table 3). The asymmetric unit consists of one CBZ and one PASA molecule (Fig. 5a). The primary interaction that holds CBZ and PASA molecules is the heterosynthon interaction ($R_2^2(8)$ ring motif) between the

Table 2 Results of LAG and slurry experiments with different pure solvents

	LAG		Slurry technique	
Solvent	(1 : 1)	(2 : 1)	(1 : 1)	(2 : 1)
Neat grinding	[CBZ + PASA] (1 : 1); CBZ	[CBZ + PASA] (1 : 1); CBZ	—	—
Acetonitrile	[CBZ + PASA] (1 : 1)	[CBZ + PASA] (1 : 1); CBZ	[CBZ + PASA] (1 : 1)	[CBZ + PASA] (1 : 1); CBZ dihyd; CBZ
Acetone	[CBZ + PASA] (1 : 1)	[CBZ + PASA] (1 : 1); CBZ	[CBZ + PASA] (1 : 1); CBZ dihyd	[CBZ + PASA] (1 : 1); CBZ dihyd; CBZ
Methanol	[CBZ + PASA] (1 : 1)	[CBZ + PASA + MeOH] (2 : 1 : 1)	[CBZ + PASA] (1 : 1)	[CBZ + PASA] (1 : 1); CBZ dihyd
Ethanol	[CBZ + PASA] (1 : 1)	[CBZ + PASA] (1 : 1); CBZ	[CBZ + PASA] (1 : 1)	[CBZ + PASA] (1 : 1); CBZ; PASA
Ethyl acetate	[CBZ + PASA] (1 : 1); CBZ	[CBZ + PASA] (1 : 1); CBZ	[CBZ + PASA] (1 : 1)	[CBZ + PASA] (1 : 1); CBZ
Tetrahydrofuran	[CBZ + PASA] (1 : 1)	[CBZ + PASA] (1 : 1); CBZ	[CBZ + PASA] (1 : 1)	[CBZ + PASA] (1 : 1); CBZ dihyd; CBZ
Chloroform	[CBZ + PASA] (1 : 1)	[CBZ + PASA] (1 : 1); CBZ	[CBZ + PASA] (1 : 1); CBZ dihyd; CBZ	[CBZ + PASA] (1 : 1); CBZ
Water	[CBZ + PASA] (1 : 1)	[CBZ + PASA] (1 : 1); CBZ; CBZ dihyd	[CBZ + PASA] (1 : 1); CBZ dihyd; CBZ	[CBZ + PASA] (1 : 1); CBZ

CBZ dihyd – dihydrate form of carbamazepine (CSD refcode FEFNOT04).[29]

carboxamide group of CBZ and the acid group of PASA *via* N–H···O (2.01(2) Å, 165(2)°) and O–H···O (1.60(2) Å, 167(2)°) hydrogen bonds. The resulting two-component supramolecular units then interact with each other *via* the N–H···O (2.22(2) Å, 163(2)°) hydrogen bond among PASA molecules to form a zigzag chain along the *b*-axis with a *C*(6) graph set notation (Fig. 5b).[30,31] The *anti*-oriented NH amide H11 atom of CBZ is not involved in any strong hydrogen bonding.

Interestingly, the crystal packing of [CBZ + PASA] (1 : 1) is significantly different from the crystal packing of a known CBZ cocrystal with PABA in a 1 : 1 molar ratio (CSD refcode XOXHEY).[24] This is due to the fact that the PASA molecule has an additional –OH group functioning as an H-bond donor (intramolecular hydrogen bond, O3–H3···O1 (1.70(2) Å, 152(2)°) and an acceptor (intermolecular hydrogen bond, N1–H1···O3 (2.22(2) Å, 163(2)°) simultaneously in contrast with the PABA molecule.

Carbamazepine/*para*-aminosalicylic acid 2 : 1 cocrystal hydrate (2). The colorless block-shaped crystals grown from ethyl acetate and acetonitrile (Table 1) belong to the monoclinic, $P2_1/n$ space group (Table 3). The asymmetric unit contains two CBZ molecules and one molecule each of PASA and water (Fig. 6a). In this case, the crystal structure of [CBZ + PASA + H_2O] shows the same packing arrangement as that of the carbamazepine cocrystal monohydrate with PABA in a 2 : 1 molar ratio (CSD refcode XAQREN).[32] The crystal structure of [CBZ + PASA + H_2O] forms an 8-membered supramolecular discrete unit consisting of four carbamazepine molecules, two *para*-aminosalicylic acid molecules and two water molecules (Fig. 6b). Carbamazepine does not form a carboxylamide heterosynthon with PASA due to the incorporation of water molecules in the crystal structure. Instead, the molecules of 2 form two types of trimeric ring motifs with $R_3^3(10)$ and $R_3^3(8)$ graph set notations. The fist trimer ($R_3^3(10)$) is composed of one molecule each of carbamazepine, *para*-aminosalicylic acid and water, in which the strongest O2–H2···O5 (1.66(2) Å, 174(2)°), between PASA and H_2O molecules) hydrogen bond in the structure (2) is realized. The

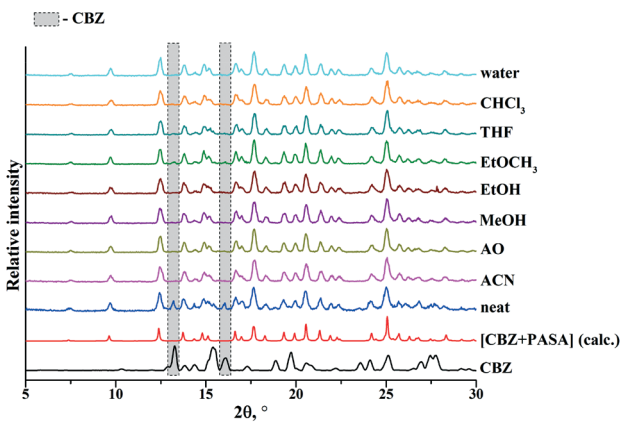

Fig. 3 XRPD patterns of the 1 : 1 CBZ and PASA mixtures obtained by grinding with different solvents.

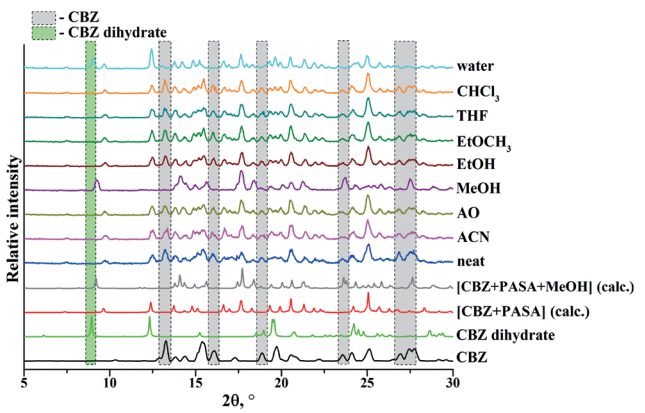

Fig. 4 XRPD patterns of the 2 : 1 CBZ and PASA mixtures obtained by grinding with different solvents.

Table 3 Crystallographic data for carbamazepine cocrystals with 4-aminosalicylic acid

	1	2	3
	[CBZ + PASA] (1 : 1)	[CBZ + PASA + H_2O] (2 : 1 : 1)	[CBZ + PASA + MeOH] (2 : 1 : 1)
CCDC no.	1544195	1544196	1544197
Chemical formula	$C_{15}H_{12}N_2O{\cdot}C_7H_7NO_3$	$2(C_{15}H_{12}N_2O){\cdot}C_7H_7NO_3{\cdot}H_2O$	$2(C_{15}H_{12}N_2O){\cdot}C_7H_7NO_3{\cdot}CH_4O$
Formula weight	389.40	643.68	657.71
Crystal structure	Monoclinic	Monoclinic	Monoclinic
Space group	$C2/c$	$P2_1/n$	$P2_1/c$
Crystal size, mm	0.30 × 0.20 × 0.20	0.30 × 0.30 × 0.20	0.40 × 0.25 × 0.20
a, Å	27.427(5)	13.6727(12)	12.6443(18)
b, Å	7.6402(15)	17.6172(15)	7.5232(11)
c, Å	21.038(4)	14.836(13)	34.674(5)
β, °	119.263(2)	116.334(1)	96.811(3)
Unit cell volume, Å^3	3845.8(13)	3202.8(5)	3275.1(8)
No. of formula units per unit cell, Z	8	4	4
D_{calc}, g cm^{-3}	1.345	1.335	1.334
T, K	150(2)	150(2)	183(2)
Absorption coefficient, μ, mm^{-1}	0.094	0.092	0.092
Data collection			
No. of reflections measured	20 588	32 373	24 975
No. of independent reflections	5123	7715	6390
Reflections with $I > 2\sigma(I)$	4512	6313	5050
R_{int}	0.0199	0.0271	0.0379
Θ_{max}, °	29.00	28.00	26.00
Refinement			
No. of parameters	338	565	583
R_1 values ($I > 2\sigma(I)$)	0.0385	0.0382	0.0377
wR^2 values (all data)	0.1058	0.1026	0.0915
Goodness of fit on F^2	1.054	1.026	1.012
Largest diff peak and hole, e Å^{-3}	0.342/−0.214	0.255/−0.255	0.191/−0.187

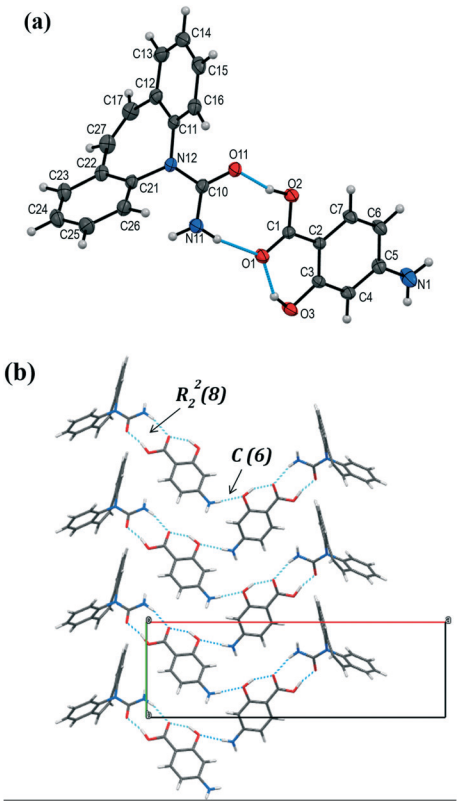

Fig. 5 (a) Asymmetric unit in [CBZ + PASA] (1 : 1). The displacement ellipsoids are shown at the 50% probability level. (b) Molecular packing projection for [CBZ + PASA] (1 : 1).

second trimer ($R_3^3(8)$) is composed of two carbamazepine molecules and one methanol molecule. As in [CBZ + PASA], the

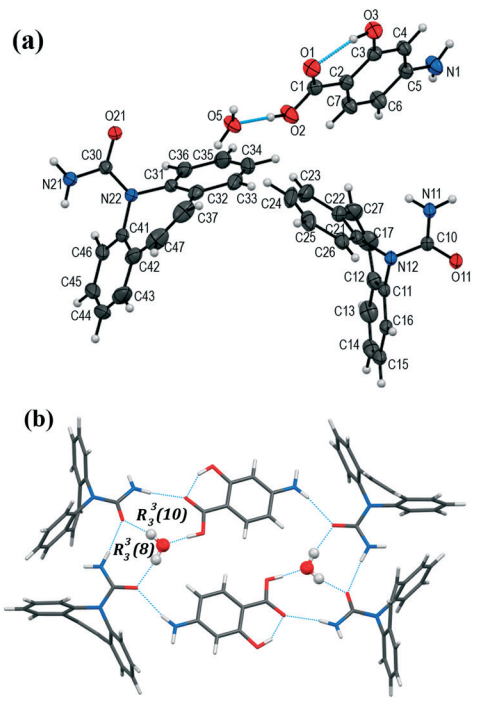

Fig. 6 (a) Asymmetric unit in [CBZ + PASA + H_2O] (2 : 1 : 1). The displacement ellipsoids are shown at the 50% probability level. (b) Discrete hydrogen bonded packing unit in [CBZ + PASA + H_2O] (2 : 1 : 1).

anti-oriented NH amide H11 and H21 atoms are not involved in any hydrogen bonding.

Carbamazepine/*para*-aminosalicylic acid 2:1 cocrystal MeOH solvate (3). The colorless block-shaped crystals grown from methanol in a 1:1 molar ratio (Table 1) belong to the monoclinic, $P2_1/c$ space group (Table 3). The asymmetric unit contains two CBZ molecules, one PASA molecule and one methanol molecule (Fig. 7).

Analysis of the packing diagram of the [CBZ + PASA + MeOH] cocrystal reveals that the structure is made up of hydrogen bonded tetramers (Fig. 8a). The hydrogen bonding motif is described by a carboxamide dimer between crystallographically different molecules of carbamazepine with an additional bent N11–H11 (*anti*-oriented)···O2 (2.59(2) Å, 126.4(1)°) hydrogen bond from CBZ to PASA and an O4–H41···O21 (1.78(2) Å, 161(2)°) hydrogen bond from methanol to CBZ. *para*-Aminosalicylic acid and methanol molecules are connected to each other *via* the strongest O2–H2···O4 (1.66(2) Å, 177(2)°) interaction in the structure (3). The hydrogen bonded tetramers form a layer along the *a*-axis *via* the N1–H1···O11 (2.17(2) Å, 156(2)°) hydrogen bond between the PASA and CBZ molecules. The neighboring layers are linked by the weak N1–H10···O3 (2.43(2) Å, 166(2)°) interaction between the PASA molecules forming a 2D structure along the *b*-axis (Fig. 8b).

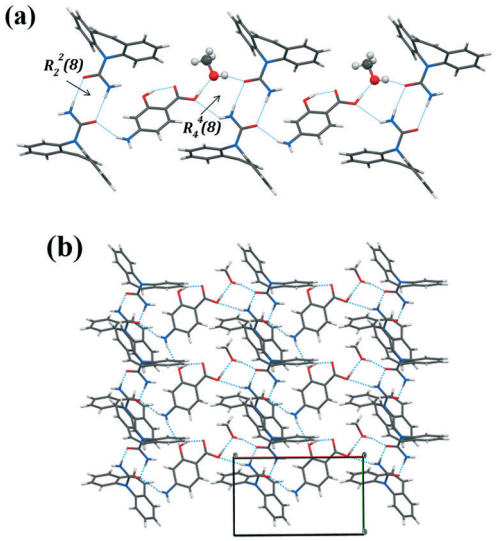

Fig. 8 (a) Layer formed by hydrogen bonded tetramers and (b) packing diagram of [CBZ + PASA + MeOH] (2:1:1).

Conformational analysis of polymorphs of CBZ and its cocrystals

CBZ is an excellent example of crystal polymorphism, wherein the conformation and the network of strong hydrogen bonds remain unchanged in all its forms. The differences between the crystal forms lie solely in the packing of the carboxamide dimer units.[23] An exception is the fifth CBZ polymorph for which the hydrogen bond network changes from the dimer motif to the catemeric hydrogen bond.[33] Moreover, the molecules in CBZ form III were found to exist in two forms that differ only in the relative orientation of the carboxamide moiety (Fig. S3, see the ESI‡).[34]

The molecule conformation of CBZ can be defined in terms of the torsion angle τ (∠C21–N12–C10–O11, Fig. 1) and one dihedral angle β between the two rings (Fig. 9) which is responsible for the mutual orientation of the different phenyl rings R_1 and R_2. The overlay of the CBZ molecular conformations in the polymorphic forms is shown in Fig. S4 (see the ESI‡), which confirms that CBZ is a conformationally rigid molecule. And, in the case of polymorphic forms, the dihedral and torsion angles remain practically the same.

In order to investigate the conformational preferences of the CBZ molecule cocrystals, a search of the CSD (v 5.36, May 2015 update)[35] for crystal structures of CBZ cocrystals was performed. The search constraints were as follows: 3D coordinates were determined; only organics; no powder structures; not disordered; $R \leq 0.1$. As a result, 40 hits, including cocrystals and their hydrates and solvates were retrieved and analyzed. The distribution of the torsion angle and the dihedral angle between the two rings from the retrieved CSD set is presented in Fig. 10a and b. The values of the selected torsion and dihedral angles for the CBZ molecule in all polymorphic forms and in all cocrystals are collected in Table S2 (see the ESI†).

As previously noted, CBZ is a rather rigid molecule. This CBZ feature is also traced in its cocrystals. The torsion angle value of the carboxamide moiety of the CBZ molecule most often ranges from 175 to 179°, which is the closest to the torsion angle value of CBZ form III. This immobility of the functional group can be explained by the fact that it is stabilized *via* the carboxamide homosynthon or the acid-amide heterosynthon in cocrystals. The torsion angle values decrease to 160–165° in cases where rather strong N–H···O or O–H···O

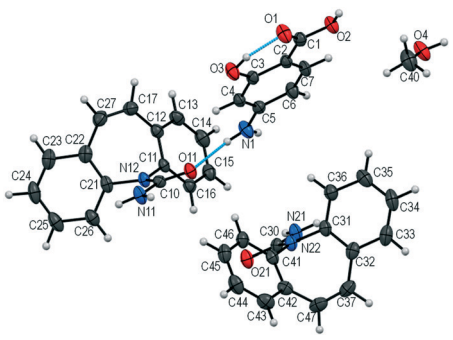

Fig. 7 Asymmetric unit in [CBZ + PASA + MeOH] (2:1:1). The displacement ellipsoids are shown at the 50% probability level.

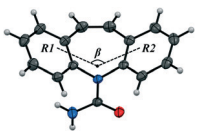

Fig. 9 Dihedral angle between the CBZ benzene rings (R_1 and R_2).

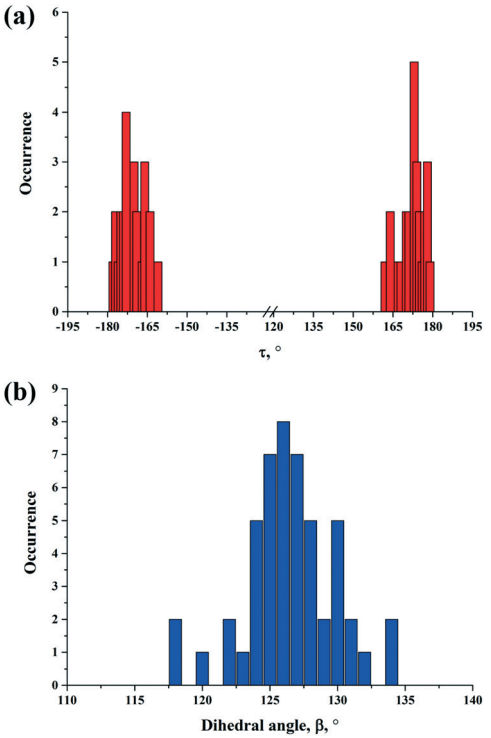

Fig. 10 (a) Distribution of torsion, τ, and (b) dihedral angle between benzene rings, β, in CBZ polymorphs, cocrystals and cocrystal solvates/hydrates retrieved from the CSD set (40 hits).

anti-oriented hydrogen bonds are formed (CBZ cocrystals with saccharin,[36] nicotinamide,[36] *para*-aminobenzoic acid[24] or adamantine-1,3,5,7-tetracarboxylic acid[36]).

Most of the structures are located between 124° and 126° dihedral angle values. The smallest dihedral angle for the CBZ molecule (119.6°) is observed in the CBZ cocrystal with isonicotinamide form I (refcode LOFKIB[37]). Such a significant alteration is explained by the formation of strong π–π interactions between the CBZ benzene ring and the isonicotinamide molecule, which are located approximately 3.8 Å apart. Moreover, the PABA and PASA cocrystal hydrates are characterized by the minimum β values. The deviation from the optimal geometry of the CBZ molecule is explained by the influence of the supramolecular environment. These cocrystal hydrates are characterized by the same packing arrangement type: the 8-membered supramolecular discrete unit consists of four carbamazepine molecules, two *para*-aminosalicylic acid molecules and two water molecules. The different discrete units "rest" on dibenzazepine fragments of CBZ, which leads to an additional stress and the "unfolding" of two benzene rings.

Crystal lattice energy calculation

The intermolecular interaction energies in the studied CBZ cocrystals with stoichiometry (1 : 1) were analyzed according to the PIXEL approach developed by Gavezzotti.[19] The calculation results are summarized in Table 4.

The calculations show that the total lattice energy for [CBZ + PASA] is *ca.* 11 kJ mol^{-1} less stabilizing than that for the [CBZ + PABA] cocrystal. The stability decrease is most likely a consequence of the presence of an intramolecular hydrogen bond in the PASA molecule, which affects the structure-forming intermolecular hydrogen bond energy in the acid-amide heterosynthon between PASA and CBZ. The same is observed for other benzoic acid derivatives. Comparing the total lattice energy in the series benzoic acid, salicylic acid, 4-hydroxybenzoic acid, PABA and PASA coformers, we can see that an increase in the number of hydrogen bond donors and acceptors leads to an increase in the total crystal lattice energy. Cocrystals with PASA and salicylic acid are exceptions due to the presence of an intramolecular hydrogen bond in the coformer molecules. The total lattice energy for [CBZ + salicylic acid] is lower than those of both the CBZ cocrystal with the structural isomer [salicylic acid + 4-hydroxybenzoic acid] (more than 20 kJ mol^{-1}) and the cocrystal [CBZ + benzoic acid] (at 7.2 kJ mol^{-1}).

However, PIXEL gives an opportunity not only to estimate the total lattice energy of the studied systems but also to partition the total energy into electrostatic, polarization, dispersion and repulsion terms. Table 4 shows that the dispersion

Table 4 Results of PIXEL calculations (kJ mol^{-1}): lattice energies (E_{latt}), Coulombic (E_{coul}), polarization (E_{pol}), dispersion (E_{disp}) and repulsion (E_{rep}) terms

	Ref.	E_{coul}	E_{pol}	E_{disp}	E_{rep}	E_{latt}
[CBZ + PASA]	[tw]	−184.4	−83	−227	217.4	−277
[CBZ + HQ]	38	−175.6	−83.8	−226	216.4	−269
[CBZ + BA]	39	−123.6	−54.8	−217.6	151.6	−244.6
[CBZ + SA]	39	−137.4	−55.8	−210.8	166.6	−237.4
[CBZ + 4-OHBA] form A	39	−193	−89.2	−228.6	236.2	−274.8
[CBZ + 4-OHBA] form C	39	−191.6	−81	−226.4	217.6	−281.2
[CBZ + PABA]	24	−196.6	−89.8	−243.2	240.4	−289.2
[CBZ + NAM]	36	−131.2	−48.2	−222.8	135.4	−266.8
[CBZ + iNAM] form A	37	−148.8	−54.6	−233.4	168.6	−268.2
[CBZ + iNAM] form B	40	−132.6	−51	−214.6	135.8	−262.4
[CBZ + Schr] form A	36	−136.2	−53.2	−248.8	151	−287.2
[CBZ + Schr] form B	41	−148.8	−61.2	−237	167.8	−279.4
[CBZ + GltAc]	39	−216.6	−97.8	−222.4	255.8	−281

HQ – Hydroquinone; BA – benzoic acid; SA – salicylic acid; 4-OHBA – 4hydroxybenzoic acid; NAM – nicotinamide; iNAM – isonicotinamide; Schr – saccharin; GltAc – glutaric acid.

interactions dominate the structures of the cocrystals, while the Coulombic term also contributes significantly to the lattice energies, particularly in [CBZ + PASA].

The maximum difference between the dispersion and Coulombic terms is observed in the [CBZ + benzoic acid], [CBZ + salicylic acid] and [CBZ + nicotinamide] cocrystals, which are characterized by the formation of separate clusters of dimers (discrete units) not bound by hydrogen bonds to the adjacent rows of cocrystal molecules. The minimum difference between the dispersion and Coulombic terms and, as a consequence, the maximum contribution of electrostatic interactions are observed in the [CBZ + glutaric acid] cocrystal with the biggest number of strong hydrogen bonds (5) attributable to the molecules of coformers. In [CBZ + 4-hydroxybenzoic acid] cocrystal form A, there are also 5 unique hydrogen bonds on two coformer molecules, but there is no acid-amide heterosynthon.

Table 5 shows the sums of the intermolecular interaction energies between the different types of molecules. In most cases, the CBZ–CF interactions make the largest contribution to the lattice energy (more than 50%). The maximum contribution of such interactions to the crystal lattice energy is found for the CBZ cocrystals with benzoic acid derivatives. The CBZ–CBZ interactions comprise approximately a third of the total energy, while less than 20% is left for the interaction between the CF molecules.

A similar relation between the CBZ–CBZ and CBZ–CF relative contributions to the total energy (*ca.* 35/55%) is observed in the CBZ cocrystals with benzoic acid derivatives. It seems that this fact can be attributed to the similarity of the packing arrangements of the considered cocrystals.

The contributions of CBZ–CBZ and CF–CF interactions are enhanced, while the contribution from CBZ–CF interactions is reduced to 40–45% for the systems where the acid-amide heterosynthon between the coformers is not realized, as well as for the systems with nicotinamide and isonicotinamide.

Thermal analysis

The DSC curves of [CBZ + PASA] (1 : 1), [CBZ + PASA + H_2O] (2 : 1 : 1) and [CBZ + PASA + MeOH] (2 : 1 : 1) are presented in Fig. 11. The melting points of the studied cocrystals and their individual components are summarized in Table 6.

The DSC curves of CBZ, PASA and [CBZ + PASA] (1 : 1) show one endotherm which corresponds to the melting process, whereas no other phase transitions are observed. The melting temperature of the [CBZ + PASA] cocrystal is found to be *ca.* 15 °C higher than the PASA one. The melting temperature values of [CBZ + PASA] [1 : 1] and [CBZ + PASA] (2 : 1) after desolvation are equal within the experimental error.

For [CBZ + PASA + H_2O] (2 : 1 : 1), the desolvation process is registered by TG at the desolvation onset temperature equaling 81.9 °C (Fig. S5, see the ESI‡).

The binding strength of the solvent in the cocrystal solvate and hydrate can be estimated by calculating the vaporization enthalpy (ΔH_S) of the cocrystal-bound solvent using the following relationship:[42,43]

$$\Delta H_S = (\Delta H^T_{desolv} \cdot 100/\Delta m_S) \cdot M_S \quad (1)$$

where ΔH^T_{desolv} is the desolvation enthalpy determined from the DSC data, Δm_S is the mass loss percent measured in the TGA experiment, and M_s is the solvent molecular weight. The resulting ΔH_S values are shown in Table 6.

The ΔH_S value for [CBZ + PASA + H_2O] indicates 45% (59.3 kJ mol^{-1}) stronger interactions of water with the host structure than pure water (40.66 kJ mol^{-1}). The enthalpy of pure methanol vaporization (35.21 kJ mol^{-1}) is found to be *ca.* 18.5 kJ mol^{-1} lower than the ΔH_S value in the solvate cocrystal. The binding strength of the solvent molecules depends on different factors, such as the packing arrangement of the host structure, the solvent accommodation, *etc.* In the case of the hydrate under investigation, the differences in ΔH_S values correlate well with the hydrate crystal structure features. The water molecules in the cocrystal hydrate interact with three neighboring coformer molecules forming the three strongest hydrogen bonds of the system: O2–H2···O5 (1.66 Å), O5–H52···O21 (1.78 Å) and O5–H51···O11 (1.91 Å). Similarly, the methanol molecules in [CBZ + PASA + MeOH] are bound to the coformers by strong hydrogen bonds, but there are only two such bonds: O2–H2···O4 (1.66 Å) and O4–H41···O21 (1.78 Å) (Table S1, see the ESI‡).

Table 5 Sums of intermolecular interaction energies (kJ mol^{-1}) between different types of molecules calculated using the PIXEL method

	CBZ–CBZ	CBZ–CF	CF–CF	Total
[CBZ + PASA]	−79.9 (28.9%)	−147.3 (53.2%)	−49.8 (18%)	−277
[CBZ + HQ]	−103.8 (38.6%)	−141.3 (52.5%)	−23.9 (8.9%)	−269
[CBZ + BA]	−84.1 (34.4%)	−139.7 (57.1%)	−20.8 (8.5%)	−244.6
[CBZ + SA]	−83.5 (35.2%)	−136.6 (57.5%)	−17.3 (7.3%)	−237.4
[CBZ + 4-OHBA] form A	−103.9 (37.8%)	−155.7 (56.7%)	−15.1 (5.5%)	−274.8
[CBZ + 4-OHBA] form C	−112.7 (40.1%)	−142.4 (50.6%)	−26.0 (9.2%)	−281.2
[CBZ + PABA]	−119.0 (41.2%)	−153.0 (52.9%)	−17.1 (5.9%)	−289.2
[CBZ + NAM]	−98.9 (37.1%)	−116.5 (43.7%)	−51.4 (19.3%)	−266.8
[CBZ + iNAM] form A	−87.5 (32.6%)	−146.7 (54.7%)	−34.0 (12.7%)	−268.2
[CBZ + iNAM] form B	−103.1 (39.3%)	−113.0 (43.0%)	−46.3 (17.6%)	−262.4
[CBZ + Schr] form A	−82.8 (28.9%)	−174.3 (60.7%)	−30.1 (10.5%)	−287.2
[CBZ +Schr] form B	−97.9 (35.0%)	−118.7 (42.5%)	−62.8 (22.5%)	−279.4
[CBZ + GltAc]	−119.4 (42.5%)	−111.4 (39.7%)	−50.3 (17.9%)	−281.0

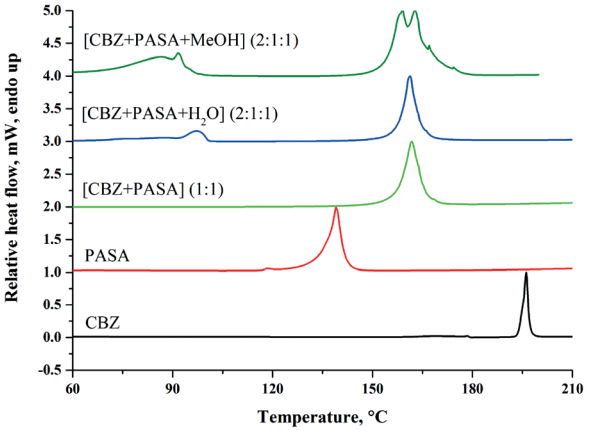

Fig. 11 DSC curves of CBZ, PASA, [CBZ + PASA] (1 : 1), [CBZ + PASA + H_2O] (2 : 1 : 1) and [CBZ + PASA + MeOH] (2 : 1 : 1) recorded at 10 °C min^{-1} heating rate.

Table 7 Temperature dependence of saturation vapor pressure and sublimation thermodynamic characteristics of carbamazepine ($P2_1/c$)[a]

T, °C	P, Pa	T, °C	P, Pa
80.0	6.10×10^{-3}	108.0	8.89×10^{-2}
81.0	6.87×10^{-3}	110.0	1.09×10^{-1}
82.0	7.45×10^{-3}	115.0	1.76×10^{-1}
83.0	8.31×10^{-3}	118.0	2.35×10^{-1}
85.0	1.02×10^{-2}	120.0	2.87×10^{-1}
90.0	1.83×10^{-2}	123.0	3.79×10^{-1}
95.0	2.93×10^{-2}	125.0	4.40×10^{-1}
100.0	4.24×10^{-2}	127.0	5.33×10^{-1}
105.0	6.72×10^{-2}	130.0	6.84×10^{-1}
ΔG^{298}_{sub}, kJ mol^{-1}	58.5	ΔS^{298}_{sub}, J mol^{-1} K^{-1}	187 ± 3
ΔH^{T}_{sub}, kJ mol^{-1}	110.9 ± 0.8	ς_H, %[c]	67.2
ΔH^{298}_{sub}, kJ mol^{-1}	114.2 ± 0.8	ς_{TS}, %[c]	32.8
$C^{298}_{p,cr}$, J mol^{-1} K^{-1}[b]	277.3	T_m, K	190.1
$T{\cdot}\Delta S^{298}_{sub}$, kJ mol^{-1}	55.7	ΔH^{T}_{fus}, kJ mol^{-1}	28.8

[a] $\ln(P[\text{Pa}]) = (32.7 \pm 0.3) - (13\,343 \pm 97)/T$; $\sigma = 3.97 \times 10^{-2}$; $r = 0.9991$; $F = 19\,078$; $n = 18$. [b] $C^{298}_{p,cr}$ has been calculated using Chickos's additive scheme;[45] the calculation procedure error corresponds to a significant digit. [c] $\varsigma_H = (\Delta H^{298}_{sub}/(\Delta H^{298}_{sub} + T{\cdot}\Delta S^{298}_{sub})){\cdot}100\%$; $\varsigma_{TS} = (T{\cdot}\Delta S^{298}_{sub}/(\Delta H^{298}_{sub} + T{\cdot}\Delta S^{298}_{sub})){\cdot}100\%$.

Cocrystal formation thermodynamics

The approach to prediction of the thermodynamic functions of cocrystal formation ($\Delta G^{0,298}_f$(CC), $\Delta H^{0,298}_f$(CC)) based on the knowledge of the melting temperatures of active pharmaceutical ingredients (API) (T_m(API)), coformers (CF) (T_m(CF)), cocrystals (T_m(CC)) and also on the sublimation Gibbs energies and enthalpies of the individual components included in the cocrystal ($\Delta G^{0,298}_{sub}$(API), $\Delta G^{0,298}_{sub}$(CF), $\Delta H^{0,298}_{sub}$(API), $\Delta H^{0,298}_{sub}$(CF)) has been developed by us earlier.[44] Literature data analysis of the sublimation thermodynamics of the individual compounds has shown that there are no sublimation data for either CBZ or PASA. If we keep in mind that CBZ is quite a common compound with a great number of cocrystals with different coformers, the study of its sublimation seems timely and relevant.

Study of CBZ sublimation. The CBZ saturation vapor pressure at different temperatures was measured by the transpiration method as described elsewhere.[21,22] The temperature dependence of the saturation vapor pressure and the calculated thermodynamic characteristics of the sublimation process are presented in Table 7. It should be noted that in the studied temperature range a thermodynamically stable modification of CBZ is form III ($P2_1/c$).[23]

Estimation of sublimation thermodynamic functions of PASA. Our sublimation experiments with PASA have failed because the substance decomposes at the experimental temperatures. Nevertheless, we tried to estimate the standard thermodynamic functions of sublimation (Gibbs energy and enthalpy) using the following approach partially described by us in 2010.[46] We have formed a database including the sublimation Gibbs energy and enthalpy of molecular crystals published up to 2016 inclusive. Moreover, the database included the melting temperatures of individual compounds. As a result, the database included 1515 molecular crystals. As we showed earlier,[46] if from the available database we select structurally related compounds based on Tanimoto similarity indices (T_c), the experimental values can be described by the correlation equation within the given group/cluster:

$$\Delta G^{0,298}_{sub} = A + B{\cdot}T_m \quad (2)$$

where the Tanimoto similarity indices (T_c) have been obtained by means of the program MOLDIVS (MOLecular DIVersity & Similarity).[47]

$$T_c = N(\text{A \& B})/[N(\text{A}) + N(\text{B}) - N(\text{A \& B})] \quad (3)$$

where N(A) is the number of fragments in molecule A, N(B) is the number of fragments in molecule B, and N(A & B) is the number of common fragments in molecules A and B.

In this program, molecular fragments are defined as atom-centered concentric environments. The fragments consist of a central atom and neighboring atoms connected to it within a predefined sphere size (the number of the bonds between the central and edge atoms). For each atom in a fragment, information on the atom and bond type, charge, valency, cycle type and size is coded into fixed-length variables which are subsequently used to define a pseudo-

Table 6 Melting (T_{fus}) and desolvation (T_{desolv}) temperatures of the CBZ cocrystal and its hydrate and solvate

	T_{desolv}, °C (onset)	ΔH^{T}_{desolv}, J g^{-1}	Δm_S, %	T_{fus}, °C (onset)	ΔH^{T}_{fus}, kJ mol^{-1}	ΔH_S, kJ mol^{-1}
[CBZ + PASA] (1 : 1)	—	—	—	154.0 ± 2.1	77.8	—
[CBZ + PASA + H_2O] (2 : 1 : 1)	81.9	72.4	2.20	154.5 ± 0.8	136.7	59.3
[CBZ + PASA + MeOH] (2 : 1 : 1)	74.7	76.5	4.56	150.8 ± 3.0	103.5	53.7

Table 8 Cocrystals selected for estimation of formation thermodynamics and their some characteristics[a]

N	API	Coformer (CF)	Ref	Stoich	T_m (API), °C	T_m (CF), °C	T_m (CC), °C	$\Delta G_{sub}^{0,298}$(API), kJ mol^{-1}	$\Delta H_{sub}^{0,298}$(API), kJ mol^{-1}	$\Delta G_{sub}^{0,298}$(CF), kJ mol^{-1}	$\Delta H_{sub}^{0,298}$(CF), kJ mol^{-1}
1	CBZ	4,4′-Bipyridine	32	2 : 1	190.1	111.8	159.0	58.5	114.20	33.6	106.3
2	CBZ	Hydroquinone	38	1 : 1	190.1	173.5	168.1	58.5	114.20	43.8	103.9
3	CBZ	Benzoic acid	13	1 : 1	190.1	122.0	112.5	58.5	114.20	34.4	90.5
4	CBZ	Malonic acid	13	1 : 1	190.1	136.0	143.4	58.5	114.20	46.7	111.4
5	CBZ	Malonic acid	48	2 : 1	190.1	134.0	142.0	58.5	114.20	46.7	111.4
6	CBZ	Adipic acid	13	1 : 1	190.1	152.0	136.8	58.5	114.20	57.5	129.3
7	CBZ	4-OHBA (form A)	13	1 : 1	190.1	213.0	171.5	58.5	114.20	55.0	113.3
8	CBZ	4-OHBA (form C)	13	1 : 1	190.1	213.0	170.0	58.5	114.20	55.0	113.3
9	CBZ	Fumaric acid	13	1 : 1	190.1	287.0	188.7	58.5	114.20	26.1	123.9
10	CBZ	Trimesic acid	36	1 : 1	190.1	375.0	278.0	58.5	114.20	100.2	159.4
11	CBZ	Glutaric acid	48	1 : 1	190.1	97.7	125.9	58.5	114.20	49.1	119.8
12	CBZ	Glutaric acid	49	2 : 1	190.1	98.0	125.0	58.5	114.20	49.1	119.8
13	CBZ	Succinic acid	48	2 : 1	190.1	188.1	188.9	58.5	114.20	58.0	123.2
14	CBZ	Salicylic acid	48	1 : 1	190.1	160.9	160.1	58.5	114.20	38.5	96.6
15	CBZ	Nicotinamide	49	1 : 1	190.1	130.6	160.0	58.5	114.20	49.0	111.8
16	CBZ	Urea	49	1 : 1	190.1	133.0	169.0	58.5	114.20	44.5	89.0
17	CBZ	Cinnamic acid	50	1 : 1	190.1	133.5	144.0	58.5	114.20	43.8	107.1
18	CBZ	PASA	tw	1 : 1	190.1	139.1	154.0	58.5	114.20	48.7	113.6
19	CBZ	PASA	tw	2 : 1	190.1	139.1	154.5	58.5	114.20	48.7	113.6

[a] T_m (API), T_m (CF), T_m (CC) are the melting temperatures of the active pharmaceutical ingredient, coformer and cocrystal, respectively; $\Delta G_{sub}^{0,298}$(API), $\Delta H_{sub}^{0,298}$(API), $\Delta G_{sub}^{0,298}$(CF), $\Delta H_{sub}^{0,298}$(CF) are the sublimation Gibbs energies and enthalpies of the active pharmaceutical ingredient and coformer; the bold values correspond to the sublimation Gibbs energy and enthalpy predicted by the clusterization approach (see text).

random hash value for this fragment. The program permits an estimation of the similarity of each molecule in the database to all the other molecules by sorting them according to the value of similarity to the initial molecule.

We have formed a cluster for PASA including the structurally related compounds selected by the criterion $0.4 < T_c$. Fig. S6 (see the ESI‡) illustrates the experimental values ΔG_{sub}^{298} for cluster elements *versus* T_m described by the correlation equation:

$$\Delta G_{sub}^{0,298} = -(23.4 \pm 5.5) + (0.175 \pm 0.012)\cdot T_m$$
$$R = 0.9119;\ \sigma = 4.08;\ n = 44 \quad (4)$$

On the other hand, we can estimate $\Delta H_{sub}^{0,298}$(PASA) using the equation relating the sublimation enthalpies and Gibbs energies of molecular crystals in a cluster (the so-called "compensation" effect). Fig. S7 (see the ESI‡) illustrates this dependence for the PASA cluster, which can be described by the equation:

$$\Delta H_{sub}^{0,298} = (52.2 \pm 3.7) + (1.26 \pm 0.07)\cdot\Delta G_{sub}^{0,298}$$
$$R = 0.9469;\ \sigma = 4.25;\ n = 44 \quad (5)$$

It is easy to estimate the thermodynamic functions of the PASA sublimation: $\Delta G_{sub}^{0,298}$(PASA) = 48.7 kJ mol^{-1} and $\Delta H_{sub}^{0,298}$(PASA) = 113.6 kJ mol^{-1}, using eqn (4) and (5) and knowing the melting point (T_m(PASA) = 412.2 K).

Formation thermodynamics of CBZ-based cocrystals. We have analyzed literature data (up to 2016) describing/confirming the crystal structures of CBZ cocrystals (single crystal X-ray or XRPD) and the cocrystal melting points. At the next stage, we used our database including the literature data on Gibbs energies and sublimation enthalpies of molecular crystals of individual compounds in order to select CBZ cocrystals with known sublimation thermodynamic functions for coformers. Table 8 lists the selected CBZ cocrystals together with the data on melting points and thermodynamic functions of the sublimation processes. Moreover, Table 8 contains the estimated values of the thermodynamic sublimation functions for PASA.

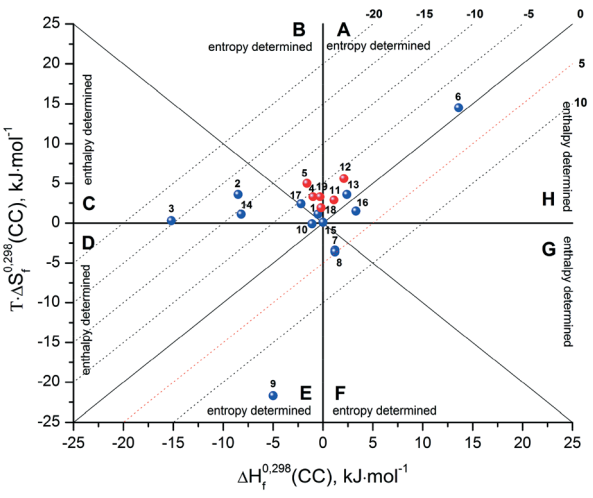

Fig. 12 Thermodynamic functions of cocrystal formation processes in coordinates of entropy term *vs.* enthalpy. The isoenergetic curves of the ΔG_f^0 function are marked by dotted lines. The numbering of the cocrystals corresponds to that in Table 8. The red points correspond to the cocrystals with the same composition but different stoichiometry (see text).

Table 9 Results of dissolution studies of pure CBZ and its cocrystal in pH 7.4 media at 25 ± 0.1 °C

	C_{max},[a] mol l^{-1}	Equilibrium solubility,[b] mol l^{-1}	Solid phase recovered after solubility experiment[c]
CBZ	$9.94 \times 10^{-4} \pm 5.79 \times 10^{-5}$	$4.77 \times 10^{-4} \pm 2.23 \times 10^{-7}$	CBZ dihyd
[CBZ + PASA] (1 : 1)	$7.68 \times 10^{-4} \pm 4.75 \times 10^{-5}$	$6.69 \times 10^{-4} \pm 1.08 \times 10^{-5}$	CBZ + CBZ dihyd + cocrystal

[a] Is the maximum concentration of CBZ in solution. [b] Is the equilibrium solubility after 6 hours of the experiment. [c] The residual materials were identified by XRPD analysis (Fig. S8, see the ESI).

Based on the approach developed by us,[44] we calculated the thermodynamic functions of the cocrystal formation. The results of the calculations are presented in Fig. 11 as a diagram, where the abscissa corresponds to the formation enthalpy ($\Delta H_f^{0,298}$), and the ordinate corresponds to the entropic term ($T\Delta S_f^{0,298}$). The dotted lines correspond to the isoenergetic cocrystal formation Gibbs energy values $\Delta G_f^{0,298}$. The diagram is divided into eight sectors, each corresponding to a different ratio of the enthalpy and entropy contributions to the Gibbs energy. Each sector is formed by two lines: on one side – the line corresponding to the zero $\Delta H_f^{0,298}$ or $T\Delta S_f^{0,298}$-value; on the other side – the bisector of the angles formed at the intersection of the coordinates ($\Delta H_f^{0,298}$; $T\Delta S_f^{0,298}$). The isoenergetic curves of Gibbs energy are marked by dotted lines. Thus, the diagram can be divided into the following areas: ($T\Delta S_f^{0,298} > \Delta H_f^{0,298} > 0$) ≡ sector **A**, ($\Delta H_f^{0,298} < 0$; $T\Delta S_f^{0,298} > 0$; $|T\Delta S_f^{0,298}| > |\Delta H_f^{0,298}|$) ≡ sector **B**, ($T\Delta S_f^{0,298} < \Delta H_f^{0,298} < 0$) ≡ sector **E**, and ($\Delta H_f^{0,298} > 0$; $T\Delta S_f^{0,298} < 0$; $|T\Delta S_f^{0,298}| > |\Delta H_f^{0,298}|$) ≡ sector **F** belonging to the entropy determined processes. The segments of the diagram where ($\Delta H_f^{0,298} < 0$; $T\Delta S_f^{0,298} > 0$; $|\Delta H_f^{0,298}| > |T\Delta S_f^{0,298}|$) ≡ sector **C**, ($\Delta H_f^{0,298} < 0$; $T\Delta S_f^{0,298} < 0$; $|\Delta H_f^{0,298}| > |T\Delta S_f^{0,298}|$) ≡ sector **D**, ($\Delta H_f^{0,298} > T\Delta S_f^{0,298} > 0$) ≡ sector **H** and (($\Delta H_f^{0,298} > 0$; $T\Delta S_f^{0,298} < 0$; $|\Delta H_f^{0,298}| > |T\Delta S_f^{0,298}|$) ≡ sector **G** correspond to the enthalpy determined processes (Fig. 12).

In our previous work,[44] we justified the selection criterion for thermodynamically stable cocrystals. This criterion claims that $\Delta G_f^{0,298} < 5$ kJ mol^{-1}, which can be explained by the possible existence of polymorphic modifications both for individual compounds and for cocrystals. Based on this criterion, eighteen out of the nineteen cocrystals selected in the literature were predicted correctly (95% correct coincidences). It should be noted that the formation of most cocrystals is an entropically controlled process: 14 cocrystals out of 19 examined. For these, the Gibbs energies of formation, as a rule, do not exceed (in modulus) the value −8 kJ mol^{-1}. In contrast, the Gibbs energies of formation are higher (in modulus) than the value −8 kJ mol^{-1} for cocrystals with entropically controlled formation (**2**, **3**, **14**).

It is interesting to compare cocrystals with identical compositions but with different stoichiometry: [CBZ + Malonic acid] (1 : 1) – (**4**) and (2 : 1) – (**5**); [CBZ + Glutaric acid] (1 : 1) – (**11**) and (2 : 1) – (**12**); [CBZ + PASA] (1 : 1) – (**18**) and (2 : 1) – (**19**). It is evident that the cocrystals with 2 : 1 stoichiometry are slightly thermodynamically more stable than similar cocrystals with 1 : 1 stoichiometry.

Dissolution experiments and stability studies

Carbamazepine is a poorly soluble drug that transforms into its dihydrate form in aqueous media, whose solubility is even worse.[51] Moreover, CBZ solubility does not depend on the change in the medium pH, since this compound is not capable of ionization. It was proved earlier that CBZ solubility can be enhanced by CBZ cocrystallization with ionizable coformers: PABA, saccharin, salicylic acid.[52,53] We used PASA as the coformer – a drug whose solubility increases with rising pH.[54] The measurements were carried out in a pH 7.4 phosphate buffer as PASA dissolves almost 9 times better than CBZ. Table 9 shows the results of the solubility experiment for both pure CBZ and its cocrystal in pH 7.4 buffer medium at 25 °C. According to the obtained data, the CBZ cocrystallization with PASA reduces the maximum CBZ concentration in the first 20 minutes but increases its equilibrium concentration, which is reached 2 hours after the start of the experiment.

Besides measuring the CBZ solubility, it was also important to check how cocrystallization affected the CBZ stability (process of hydration) in an aqueous medium. Fig. 13 illustrates that CBZ in pH 7.4 phosphate buffer begins to quickly convert into its dihydrate form after remaining in the aqueous medium for 20 minutes. This results in a sharp drop in CBZ solubility. This CBZ transformation is also confirmed by the analysis of the solid phase after the experiment (Fig. S8, see the ESI‡); its XRPD pattern coincides with the XRPD pattern of the dihydrate CBZ. In turn, cocrystallization leads to a significant deceleration of CBZ hydration, which is reflected by the absence of a characteristic peak during pure CBZ

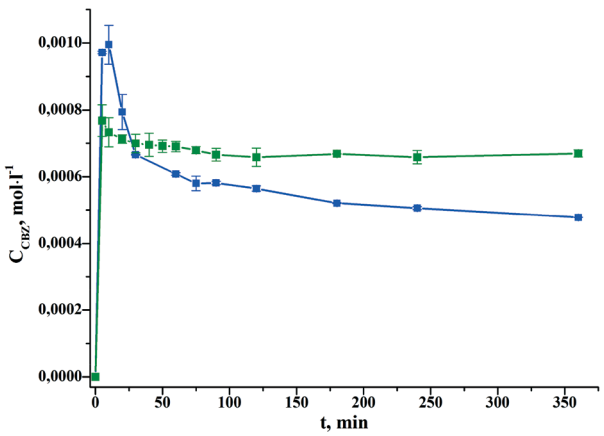

Fig. 13 Dissolution profiles of pure CBZ (■) and CBZ cocrystal (■).

dissolution. The cocrystal solid phase analysis after the experiment also confirms that after 6 hours in water, CBZ is only partly transformed into its dihydrate form. In the XRPD pattern, there are peaks related to both the dihydrate CBZ form and the unhydrated CBZ. Thus, CBZ cocrystallization with PASA leads to a significant decrease (up to several hours) of the CBZ rate of conversion from the anhydrous to the hydrate form, and as a consequence, a solubility increase of approximately 1.5 times.

Conclusions

Three new CBZ cocrystals with *para*-aminosalicylic acid, a second-line antituberculosis drug, have been prepared by both solvent-drop grinding and solution techniques. The pure [CBZ + PASA + MeOH] (2 : 1 : 1) form was obtained only by grinding of CBZ and PASA in (2 : 1) stoichiometry with the addition of methanol. [CBZ + PASA + H_2O] (2 : 1 : 1) was produced only by solution crystallization from acetonitrile and ethyl acetate.

The crystal structures of [CBZ + PASA] (1 : 1), [PASA + CBZ + H_2O] (2 : 1 : 1) and [PASA + CBZ + MeOH] (2 : 1 : 1) have been analyzed. Comparative analysis of the molecular packing in the obtained cocrystal and in a structurally related [CBZ + PABA] cocrystal has been conducted . It has been found that the presence of an additional donor and an additional acceptor of the hydrogen bond in the PASA molecule leads to the formation of an acid-amide heterosynthon with CBZ *versus* PABA. This difference significantly affects the molecular packing in the cocrystals.

We have conducted a conformational analysis of the CBZ molecule in the crystals obtained by us in this work in comparison with polymorphs of CBZ, its cocrystals and solvates described in the CSD. It has been shown that the torsion angle value of the carboxamide moiety varies between 175° and 179°, which is the closest to the torsion angle value of CBZ form III. The position of the functional group is stabilized by the carboxamide homosynthon or acid-amide heterosynthon in the cocrystals. The torsion angle value decreases to 160–165° in cases where there are strong N–H···O or O–H···O anti-oriented hydrogen bonds. Most of the structures are located between 124° and 126° dihedral angle values between the two rings.

The intermolecular interaction energies in the studied CBZ cocrystals with (1 : 1) stoichiometry were analyzed according to the PIXEL approach. The analysis of the total lattice energy values in the series of CBZ cocrystals with benzoic acid derivatives has shown that a bigger number of hydrogen bond donors and acceptors leads to an increase in the total crystal lattice energy except in compounds with an intramolecular hydrogen bond. The results of PIXEL calculations show that the dispersion interactions dominate the structures of the cocrystals, while the Coulombic term also contributes significantly to the lattice energies. The largest difference between the dispersion and Coulombic terms was observed in cocrystals characterized by the formation of separate dimer clusters not connected by hydrogen bonds with the neighboring rows of cocrystal molecules. The CBZ–CF interactions provide the largest contribution to the lattice energy (more than 50%). The contributions of CBZ–CBZ and CF–CF interactions increase, while the contribution of the CBZ–CF interactions decreases to 40–45% for systems in which the acid-amide heterosynthon is not realized.

The thermodynamic parameters of the sublimation process of carbamazepine form III were obtained for the prediction of the thermodynamic functions of cocrystal formation based on the knowledge of the melting temperatures of active pharmaceutical ingredients, coformers, and cocrystals and also on the sublimation Gibbs energies and enthalpies of individual components included in the cocrystals. The thermodynamic functions of the CBZ cocrystal formation with a number of known cocrystals were calculated. Based on the conducted calculations, eighteen out of the nineteen cocrystals selected in the analyzed literature were predicted correctly (95% correct coincidences). It has been shown that the formation of most cocrystals is an entropically controlled process (14 cocrystals out of 19 examined).

The dissolution process of the [CBZ + PASA] cocrystal (1 : 1) in pH 7.4 phosphate buffer has been studied. The cocrystallization of CBZ with PASA leads to a significant decrease (up to several hours) of the CBZ rate of conversion from the anhydrous to the hydrate form, and as a result, a CBZ solubility increase by approximately 1.5 times.

Acknowledgements

This work was supported by the Russian Foundation of Basic Research (grant No. 16-53-150007). The single crystal X-ray diffraction studies were performed at the Centre of Shared Equipment of IGIC RAS. We thank "the Upper Volga Region Centre of Physicochemical Research" for technical assistance with TGA and XRPD experiments.

Notes and references

1 X. Wan, P. Ma and X. Zhang, *Asian J. Pharm. Sci.*, 2014, **9**, 1.
2 R. Thipparaboina, D. Kumar, R. B. Chavan and N. R. Shastri, *Drug Discovery Today*, 2016, **21**, 481.
3 N. Schultheiss and A. Newman, *Cryst. Growth Des.*, 2009, **9**, 2950.
4 R. Thakuria, A. Delori, W. Jones, M. P. Lipert, L. Roy and N. Rodriguez-Hornedo, *Int. J. Pharm.*, 2013, **453**, 101.
5 FDA, *Guidance for industry*, 2011, https://www.fda.gov/downloads/Drugs/GuidanceComplianceRegulatoryInformation/Guidance1054s/UCM281764.pdf.
6 G. R. Desiraju, *Angew. Chem., Int. Ed. Engl.*, 1995, **34**, 2311.
7 R. Chadha, A. Saini, P. Arora, D. S. Jain, A. Dasgupta and T. N. G. Row, *CrystEngComm*, 2011, **13**, 6271.
8 S. Aitipamula, P. S. Chow and R. B. H. Tan, *CrystEngComm*, 2009, **11**, 1823.
9 M. L. Cheney, D. R. Weyna, N. Shan, M. Hanna, L. Wojtas and M. J. Zaworotko, *J. Pharm. Sci.*, 2011, **100**, 2172.

10 B. S. Sekhon, *Daru, J. Pharm. Sci.*, 2012, **20**, 45.
11 WHO, Expert committee on specifications for pharmaceutical preparations, *Fortieth report*, 2006, p. 402.
12 Z. Rahman, C. Agarabi, A. S. Zidan, S. R. Khan and M. A. Khan, *AAPS PharmSciTech*, 2011, **12**, 693.
13 S. L. Childs, N. Rodriguez-Hornedo, L. S. Reddy, A. Jayasankar, C. Maheshwari, L. McCausland, R. Shipplett and B. C. Stahly, *CrystEngComm*, 2008, **10**, 856.
14 M. Schiebler, K. Brown, K. Hegyi, S. M. Newton, M. Renna, L. Hepburn, C. Klapholz, S. Coulter, A. Obregon-Henao, M. Henao Tamayo, R. Basaraba, B. Kampmann, K. M. Henry, J. Burgon, S. A. Renshaw, A. Fleming, R. R. Kay, K. E. Anderson, P. T. Hawkins, D. J. Ordway, D. C. Rubinsztein and R. A. Floto, *EMBO Mol. Med.*, 2015, **7**, 127.
15 A. Swart and V. Harris, *Continuing Medical Education*, 2005, **23**, 56.
16 A. V. Yadav, A. S. Shete, A. P. Dabke, P. V. Kulkarni and S. S. Sakhare, *Indian J. Pharm. Sci.*, 2009, **71**, 359.
17 G. M. Sheldrick, *SADABS*, Program for scaling and correction of area detector data, University of Göttingen, Germany, 1997.
18 G. M. Sheldrick, *Acta Crystallogr., Sect. A: Found. Crystallogr.*, 2008, **64**, 112.
19 A. Gavezzotti, *Mol. Phys.*, 2008, **106**, 1473.
20 L. Maschio, B. Civalleri, P. Ugliengo and A. Gavezzotti, *J. Phys. Chem. A*, 2011, **115**, 11179.
21 A. N. Manin, A. P. Voronin and G. L. Perlovich, *Thermochim. Acta*, 2014, **583**, 72.
22 W. Zielenkiewicz, G. L. Perlovich and M. Wszelaka-Rylik, *J. Therm. Anal. Calorim.*, 1999, **57**, 225.
23 A. L. Grzesiak, M. Lang, K. Kim and A. J. Matzger, *J. Pharm. Sci.*, 2003, **92**, 2260.
24 A. Jayasankar, L. S. Reddy, S. J. Bethune and N. Rodrigues-Hornedo, *Cryst. Growth Des.*, 2009, **9**, 889.
25 Z. Li and A. J. Matzger, *Mol. Pharmaceutics*, 2016, **13**, 990.
26 A. V. Trask, W. D. S. Mothrwell and W. Jones, *Cryst. Growth Des.*, 2005, **5**, 1013.
27 K. Guo, G. Sadiq, C. Seaton, R. Davey and Q. Yin, *Cryst. Growth Des.*, 2010, **10**, 268.
28 S.-W. Zhang, M. T. Harasimowicz, M. M. de Villiers and L. Yu, *J. Am. Chem. Soc.*, 2013, **135**, 18981.
29 A. Kogan, I. Popov, V. Uvarov, S. Cohen, A. Aserin and N. Garti, *J. Dispersion Sci. Technol.*, 2007, **28**, 1008.
30 M. C. Etter, *Acc. Chem. Res.*, 1990, **23**, 120.
31 J. Bernstein, R. E. Davis, L. Shimoni and N.-L. Chang, *Angew. Chem., Int. Ed. Engl.*, 1995, **34**, 1555.
32 J. A. McMahon, J. A. Bis, P. Vishweshwar, T. R. Shattock, O. L. McLaughlin and M. J. Zaworotko, *Z. Kristallogr.*, 2005, **220**, 340.
33 J.-B. Arlin, L. S. Price and S. L. Price, *Chem. Commun.*, 2011, **47**, 7074.
34 T. Gelbrich and M. B. Hursthouse, *CrystEngComm*, 2006, **8**, 448.
35 F. H. Allen, *Acta Crystallogr., Sect. B: Struct. Sci.*, 2002, **58**, 380.
36 S. G. Fleischman, S. S. Kuduva, J. A. McMahon, B. Moulton, R. D. B. Walsh, N. Rodriguez-Hornedo and M. J. Zaworotko, *Cryst. Growth Des.*, 2003, **3**, 909.
37 J. H. ter Horst and P. W. Cains, *Cryst. Growth Des.*, 2008, **8**, 2537.
38 S. Aitipamula, P. S. Chow and R. B. H. Tan, *J. Chem. Crystallogr.*, 2011, **41**, 1604.
39 S. L. Childs, P. A. Wood, N. Rodriguez-Hornedo, L. S. Reddy and K. I. Hardcastle, *Cryst. Growth Des.*, 2009, **9**, 1869.
40 M. Habgood, M. A. Deij, J. Mazurek, S. L. Price and J. H. ter Horst, *Cryst. Growth Des.*, 2010, **10**, 903.
41 W. W. Porter III, S. C. Elie and A. J. Matzger, *Cryst. Growth Des.*, 2008, **8**, 14.
42 M. R. Caira, G. Bettinetti and M. Sorrenti, *J. Pharm. Sci.*, 2002, **91**, 467.
43 A. O. Surov, A. N. Manin, A. P. Voronin, K. V. Drozd, A. A. Simagina, A. V. Churakov and G. L. Perlovich, *Eur. J. Pharm. Sci.*, 2015, **77**, 112.
44 G. L. Perlovich, *CrystEngComm*, 2015, **17**, 7019.
45 J. S. Chickos and W. E. Acree Jr., *J. Phys. Chem. Ref. Data*, 2002, **31**, 537.
46 G. L. Perlovich and O. A. Raevsky, *Cryst. Growth Des.*, 2010, **10**, 2707.
47 O. A. Raevsky, V. A. Gerasimenko and S. V. Trepalin, *MOLDIVS (MOLecular DIVersity& Similarity) program package*, Registration by Russian State Patent Agency No. 990093 of 26.02.99.
48 D. J. Good and N. Rodriguez-Hornedo, *Cryst. Growth Des.*, 2009, **9**, 2252.
49 E. Lu, N. Rodriguez-Hornedo and R. Suryanarayanan, *CrystEngComm*, 2008, **10**, 665.
50 A. Shayanfar, K. Asadpour-Zeynali and A. Jouyban, *J. Mol. Liq.*, 2013, **187**, 171.
51 F. Keramathnia, A. Shayanfar and A. Jouyban, *J. Pharm. Sci.*, 2015, **104**, 2559.
52 S. J. Bethune, N. Huang, A. Jayasankar and N. Rodriguez-Hornedo, *Cryst. Growth Des.*, 2009, **9**, 3976.
53 A. Alhalaweh, L. Roy, N. Rodriguez-Hornedo and S. P. Velaga, *Mol. Pharmaceutics*, 2012, **9**, 2605.
54 K. V. Drozd, A. N. Manin, A. V. Churakov and G. L. Perlovich, *Eur. J. Pharm. Sci.*, 2017, **99**, 228.

